ACS APPLIED MATERIALS & INTERFACES

Research Article

www.acsami.org

# Defect-Driven Magnetism in Luminescent *n*/*p*-Type Pristine and Gd-Substituted $SnO_2$ Nanocrystalline Thin Films

S. Ghosh,* Gobinda Gopal Khan, and K. Mandal

Department of Condensed Matter Physics and Material Sciences, S. N. Bose National Centre for Basic Sciences, Block JD, Sector III, Salt Lake City, Kolkata 700 098, India

**ABSTRACT:** The effects of rare-earth-element Gd doping on the intrinsic magnetic ordering, photoluminescence, and electrical-conducting properties of the pristine $SnO_2$ nanocrystalline thin films fabricated by radio-frequency (RF) sputtering are investigated. The pristine $SnO_2$ thin film exhibits significant ferromagnetism while Gd doping results in an absence of intrinsic ferromagnetism. The presence of large amounts of singly ionized oxygen vacancies ($V_O^+$) is traced by photoluminescence spectroscopic analysis and they are found to be responsible for the observed ferromagnetism in pristine $SnO_2$ thin films. A significant reduction of oxygen vacancies is observed after Gd doping, and that might be insufficient to mediate long-range ferromagnetic ordering between $V_O^+$ defects in a Gd-doped $SnO_2$ system. Although the associated magnetic moment is increased by 1 order of magnitude, because of the insertion of $Gd^{3+}$ ions, which have localized *f*-shell paramagnetic moment, there is no intrinsic FM ordering. Hall measurement reveals that the pure $SnO_2$ exhibits *n*-type behavior whereas Gd-doped $SnO_2$ films show the *p*-type conductivity with higher resistivity. The studies demonstrate that only structural defects such as $V_O^+$ defects, not magnetic ions such as $Gd^{3+}$, are responsible for inducing ferromagnetism in $SnO_2$ thin films.

**KEYWORDS:** *tin dioxide, ferromagnetism, structural defects, photoluminescence, conductivity*

## 1. INTRODUCTION

The issue of magnetism in oxide semiconductor thin films has attracted immense attraction for current research, because of their considerable practical application in spin- and charge-controlled devices, which are known as spintronics.[1,2] In 2000, Dietl et al.[3] demonstrated that ferromagnetic mediation between Mn ions in *p*-type Mn-doped GaAs is possible and they have predicted the possibility of high Curie temperature ($T_c$) ferromagnetism (FM) in oxide and nitride semiconductors. Since then, large numbers of reports have appeared in the literature demanding room-temperature ferromagnetism (RTFM) in transition-metal (TM)- or rare-earth-element (RE)-doped wide-band-gap oxide semiconductors.[4−7] But still, the origin of FM in such magnetic ion-doped oxides has been greatly challenged by some scientists and eventually leads to a controversial issue about the presence or absence of FM.[8−12] Ogale et al.[13] reported FM conditions in a Co-doped $SnO_2$ thin film that had a giant magnetic moment (~7.5 ± 0.5 $\mu_B$ per Co ion). Liu et al.[14] have shown that FM in Co-doped $SnO_2$ nanocrystalline thin films is mediated by structural defects and magnetization is dependent on the thickness of films. In our earlier work, we found that Co-doped $SnO_2$ exhibits paramagnetism (PM) in bulk systems, whereas non-DMS-related FM is observed in Co-doped $SnO_2$ nanorods.[15] Recently, research also has shown the absence of FM in TM-doped oxides, with their high structural perfection.[16,17] Fernandes et al.[18] also have observed the significant loss of the ferromagnetic signature in the $CeO_2$ films upon the low level doping of the Mn, Fe, Co, and Cu ions in the matrix. Therefore, considering the controversy related to the issue of FM in magnetic ion-doped oxides, the RTFM in pure and nonmagnetic-ion-doped oxides has been investigated.[19−21] The reported RTFM in pure $HfO_2$ thin films by Venkatesan et al.[19] has opened up a new phenomenon, called $d^0$-ferromagnetism. RTFM has also been reported for pure oxides such as ZnO, $SnO_2$, and $TiO_2$.[20] The *ab initio* calculations performed by Pemmaraju et al.[22] for $HfO_2$ and by Elfimov et al.[23] for CaO have indicated that the cationic vacancies can induce an almost localized magnetic moment on the oxygen atoms neighboring the vacancy site. In our earlier work, we also have found that the FM in ZnO nanowires can be tuned by controlling Zn vacancy ($V_{Zn}$) defects using nonmagnetic potassium (K) as a dopant.[21] On the other hand, oxygen vacancies ($V_O$) have also been attributed to introducing RTFM in wide-band-gap oxide semiconductors such as ZnO, $In_2O_3$, and $SnO_2$.[20,24,25] The controlling of the FM by tuning of the oxygen vacancies is reported in the Li−Ni-codoped ZnO,[26] ZnO,[27] and Cr-doped $In_2O_3$[28,29] thin films and nanostructures.

$SnO_2$ is an important *n*-type semiconductor with remarkable optical properties, which are due to its wide band gap (~3.6 eV). During the preparation of $SnO_2$ thin films under variable conditions, different intrinsic structural defects such as Sn interstitial ($Sn_i$), oxygen vacancy ($V_O$), and Sn vacancy ($V_{Sn}$) can be generated. Among them, only the Sn vacancy ($V_{Sn}$) and singly ionized oxygen vacancy ($V_O^+$) are reported to show localized moments, whereas the other defects (such as $Sn_i$ or neutral $V_O$ or $V_O^{2+}$) are nonmagnetic.[30−32] The density functional theory (DFT) study performed by Rahman et al.[31] showed that $V_{Sn}$ can generate a large magnetic moment around 4 $\mu_B$ and they also have attributed the experimentally observed giant magnetic moment of Co-doped $SnO_2$ thin films[13] to the $V_{Sn}$ defects. Generally, it is very unlikely to have a considerable

Received: January 5, 2012
Accepted: March 16, 2012
Published: March 16, 2012

  

amount of $V_{Sn}$ defects in pure $SnO_2$ thin films due to the high formation energy of $V_{Sn}$ defects. On the other hand, oxygen vacancy ($V_O$) can easily grow during $SnO_2$ thin film deposition, because of its low formation energy.[33] However, there are limited numbers of reports about the defect magnetism in $SnO_2$ thin films, unlike ZnO. In fact, the effects of the rare-earth-element (RE)-ion doping on the magnetic properties of the $SnO_2$ thin films are still limited.[34] The doping of the RE element in the $SnO_2$ matrix can provide the exciting optical and magnetic properties of the thin films. Hence, RE-ion-doped $SnO_2$ could be interesting from the viewpoint of optical and spintronic applications. Moreover, trivalent Gd ions have larger localized magnetic moments, because of their $4f^7$ electron configuration, compared to the TM ions. Therefore, it is expected that the Gd-doped oxides could exhibit a large ferromagnetic moment and the substitution of trivalent Gd ions at the tetravalent Sn site can also introduce holes in the $SnO_2$ system, which can be favorable to sustaining FM coupling. Therefore, in this report, we have investigated the origin of FM in pristine and Gd-doped $SnO_2$ thin films coupled with their magnetic, photoluminescence, and electrical properties. We have found that singly ionized oxygen vacancies ($V_O^+$) are responsible for inducing FM in $SnO_2$ nanocrystalline thin films, whereas the Gd doping has little influence on FM in the $SnO_2$ thin films.

## 2. EXPERIMENTAL DETAILS

Pure and Gd-doped $SnO_2$ thin films have been deposited on a Si(100) substrate using a radio-frequency (RF) sputtering technique. For the preparation of the target, high-purity $SnO_2$ (99.99%) and $Gd_2O_3$ (99.99%), in the appropriate ratio, are mechanically milled using Fritsch Pulverisette-7 mill. The mixture is sintered at 800 °C for 12 h and a pallet 1 in. in diameter is prepared from it. The pallet is sintered again at high temperature (1000 °C) for 4 h. Afterward, it is used as target material for the deposition of $SnO_2$ and $Sn_{1-x}Gd_xO_2$ ($x$ = 0.02 and 0.05) thin films. The RF sputtering is conducted using a power of 50 W dc, where the ratio of argon (Ar) and oxygen ($O_2$) is 10:1. The base pressure of the sputtering chamber is $2.7 \times 10^{-2}$ mbar. The average deposition rate is ~4.5 nm/min, and the total deposition time is 45 min. Afterward, the as-deposited pure and Gd-doped $SnO_2$ films are annealed at 700 °C in an oxygen atmosphere for 3 h to improve the crystalline quality of the films. All the annealed $SnO_2$ thin films are characterized by XRD for phase identification and thicknesses of the films are measured using an ellipsometer. Scanning electron microscopy (SEM) is used to examine the surface morphology of the films. Magnetic measurements are performed by superconducting quantum interference devices (SQUIDs). Photoluminescence (PL) spectroscopic measurements are conducted to observe the defect-levels transitions between the optical band gap of $SnO_2$ thin films. Hall measurement is carried out to investigate the types ($n$-type/$p$-type) of the semiconductors and to estimate the carrier concentrations. The resistivity of films is measured with standard four-probe method with two current and voltage leads.

## 3. RESULTS AND DISCUSSION

The crystallographic phase identification of the pure and Gd-doped $SnO_2$ thin films have been performed using XRD (patterns are shown in Figure 1). All the peaks with the mentioned ($h\,k\,l$) values correspond to the tetragonal rutile structure of the $SnO_2$ lattice. Note that all the films are single phase, without the presence of any impurity phase. The peak at ~44.3° originates from the Si substrate upon which the $SnO_2$ films are deposited. The variation of the lattice parameters and $d$-spacing ($d_{110}$ and $d_{101}$) between parallel planes of $SnO_2$ unit cell, estimated using Bragg's diffraction law, are shown in

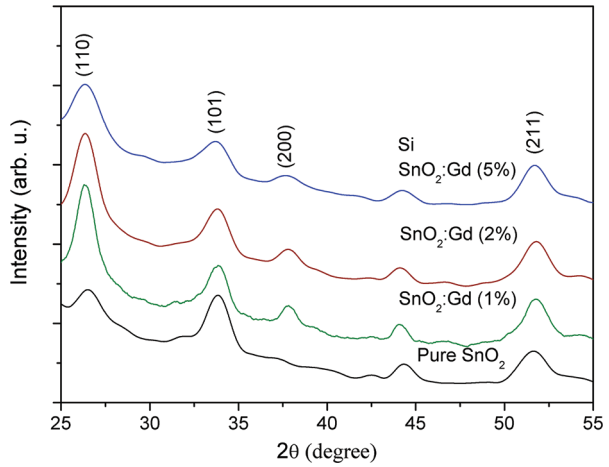


**Figure 1.** X-ray diffraction (XRD) patterns of pristine $SnO_2$ and Gd-doped $SnO_2$ thin films at room temperature (300 K).

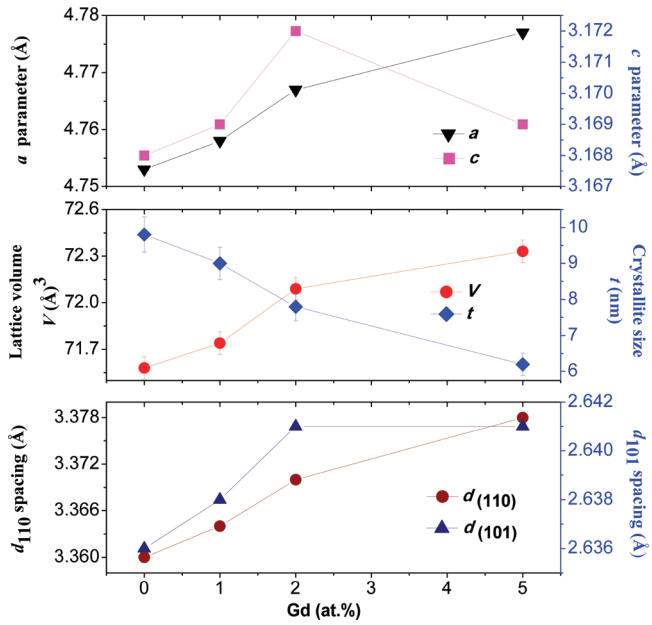


**Figure 2.** Variation of lattice parameters ($a$ and $c$), lattice volume ($V$), crystallite size ($t$), and $d$-spacing of the (110) and (101) crystal planes of $SnO_2$ lattice, relative to Gd concentration (at.%).

Figure 2. It is important to notice that the lattice parameters ($a$ ($a$ = $b$) and $c$) as well as lattice volume ($V$) are found to increase with Gd doping. This expansion of the lattice volume ensures the substitution of larger $Gd^{3+}$ ions (1.07 Å) replacing smaller $Sn^{4+}$ ions (0.69 Å) in the $SnO_2$ matrix. This type of variation of the lattice parameters is also observed for other TM-doped $SnO_2$ thin films.[10,11,14] The values of lattice parameters and $d$-spacing for different crystallographic planes of the different films are also summarized in Table 1. The full width at half-maximum (fwhm) of the (110) peak is observed to increase with increasing Gd doping, which signifies a decrease in the average crystallite sizes ($t$) of the films. The average crystallite sizes of the thin films are estimated using the Debye–Scherrer formula,

$$t = \frac{0.9\lambda}{\beta \cos\theta}$$


dx.doi.org/10.1021/am300023a | ACS Appl. Mater. Interfaces 2012, 4, 2048–2056

**Table 1. Typical Estimated Values of Lattice Parameters ($a$ and $c$), Lattice Volume ($V$), $d$-Spacing of the (110) and (101) Planes, Full Width at Half Maximum (fwhm) of the (110) Plane, and Crystallite Size ($t$) of As-Deposited Pristine and Gd-Doped $SnO_2$ Thin Films**

| | Lattice Parameters | | | $d$-Spacing (Å) | | | |
|---|---|---|---|---|---|---|---|
| thin film | $a^a$ (Å) | $c$ (Å) | volume, $V$ (Å$^3$) | $d_{110}$ | $d_{101}$ | fwhm at (110) (°) | crystallite size, $t$ (nm) |
| $SnO_2$ | 4.753 | 3.168 | 71.56 ± 0.07 | 3.360 | 2.636 | 1.85 ± 0.02 | 9.8 ± 0.3 |
| $SnO_2$:Gd (1%) | 4.758 | 3.169 | 71.74 ± 0.07 | 3.364 | 2.638 | 2.02 ± 0.02 | 9.0 ± 0.3 |
| $SnO_2$:Gd (2%) | 4.767 | 3.172 | 72.08 ± 0.07 | 3.370 | 2.640 | 2.34 ± 0.02 | 7.8 ± 0.3 |
| $SnO_2$:Gd (5%) | 4.777 | 3.169 | 72.31 ± 0.07 | 3.378 | 2.641 | 2.91 ± 0.02 | 6.3 ± 0.3 |

[a]Note that $a = b$.

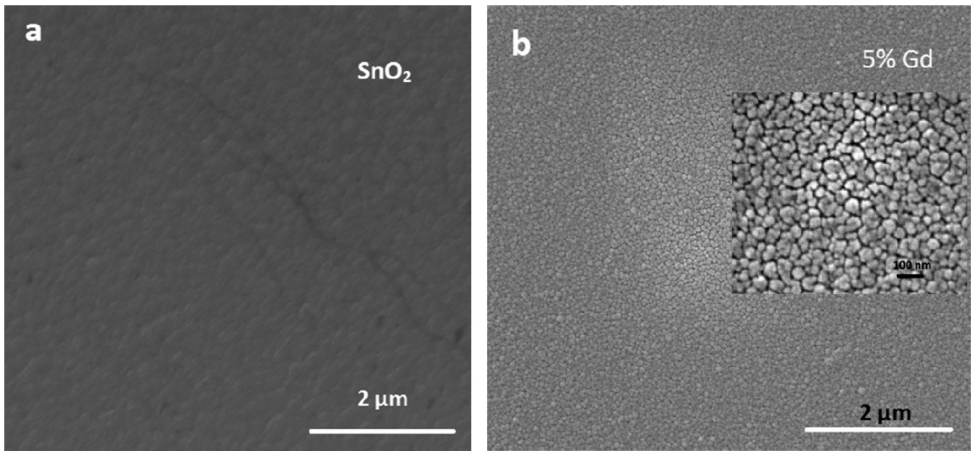


**Figure 3.** SEM images of (a) a pristine $SnO_2$ thin film and (b) a 5% Gd-doped $SnO_2$ thin film. Inset in panel b shows a high-magnification image of the corresponding thin film, revealing the nanocrystalline nature of the film.

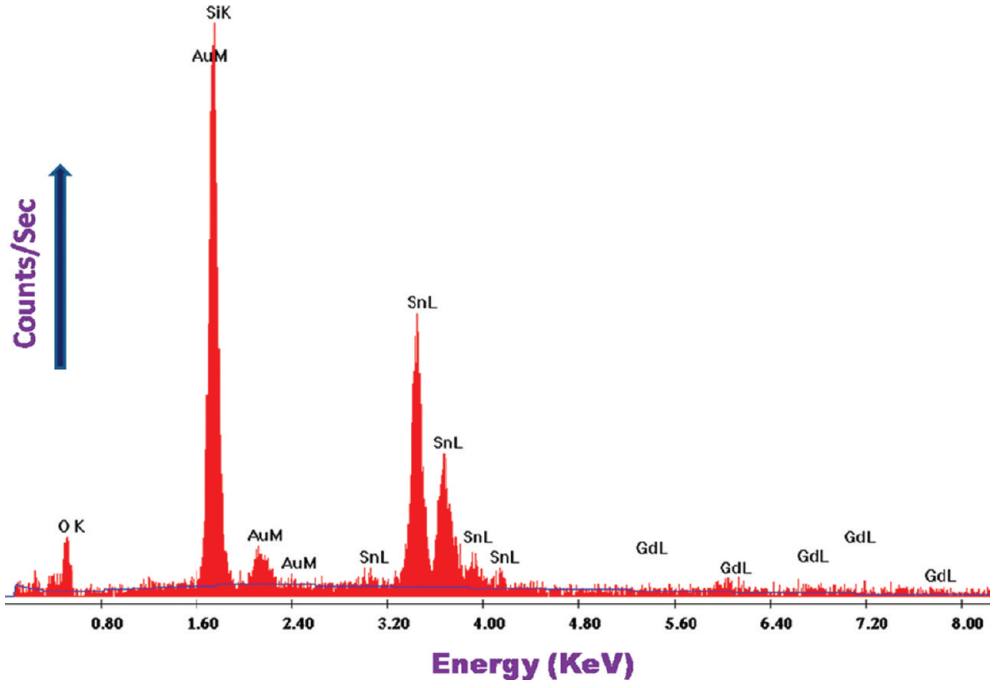


**Figure 4.** Energy-dispersive X-ray (EDAX) spectrum of the 5% Gd-doped $SnO_2$ thin film.

where $\lambda$ is the wavelength of X-ray beam used (1.54 Å for Cu K$\alpha$ radiation), $\theta$ the peak position of the given ($hkl$) peak, and $\beta$ the corresponding fwhm in radian. The average $t$ values of all thin films are found to be <10 nm, which demonstrates the nanocrystalline nature of the thin films (see Table 1). The thicknesses of the thin films measured by ellipsometer are found to be 228, 217, 210, and 205 nm for pure, 1%, 2%, and 5% Gd-doped $SnO_2$, respectively.

Figure 3 shows the low-magnification SEM images of the pure $SnO_2$ thin film (Figure 3a) and the 5% Gd-doped $SnO_2$ thin film (Figure 3b); the inset of Figure 3b shows the high-magnification image of the corresponding thin film. The SEM

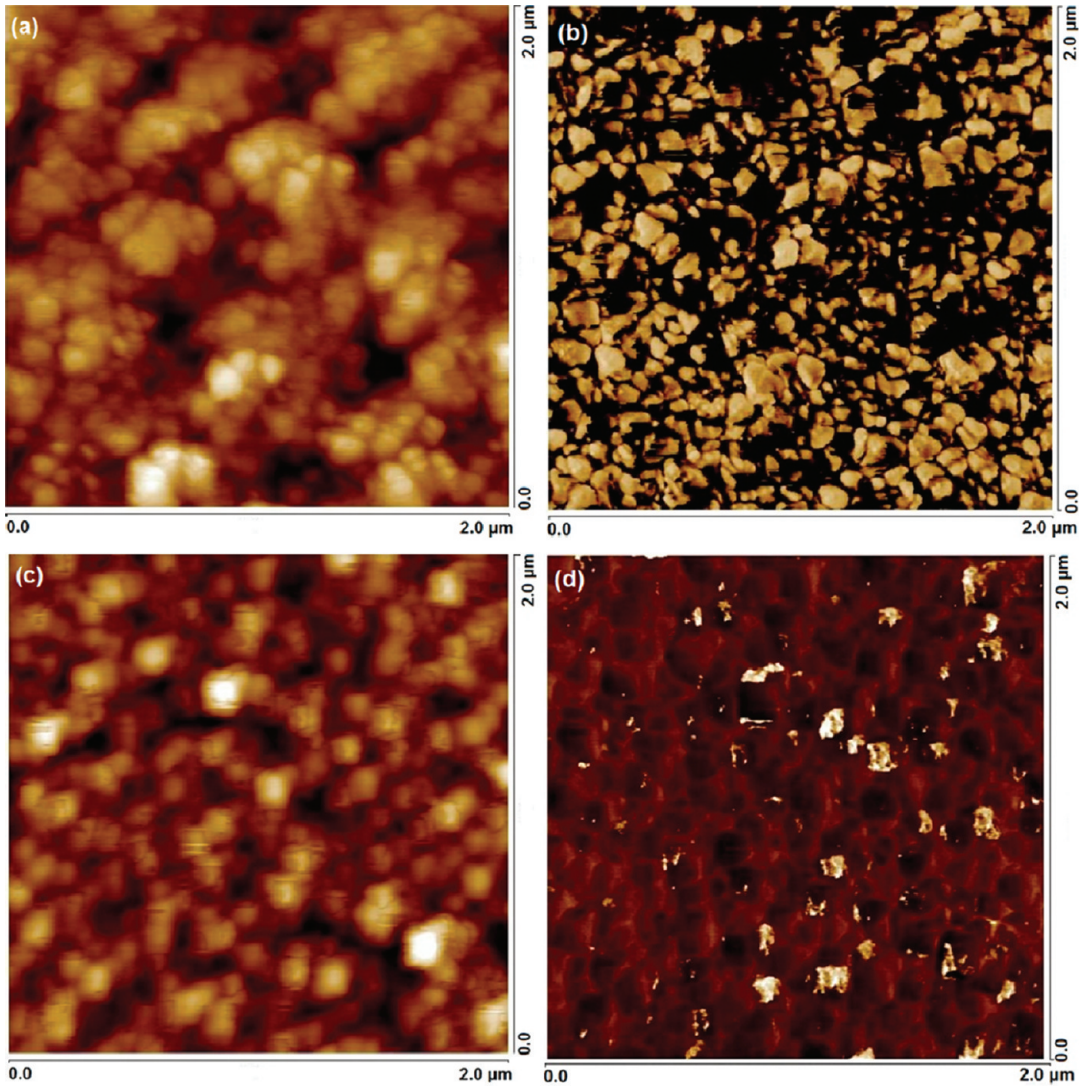


**Figure 5.** (a, c) Topographic atomic force microscopy (AFM) images and (b, d) the corresponding grainlike magnetic domain structures revealed by the magnetic force microscopy (MFM) imaging, for the pure film (panels a and b) and the 5% Gd-doped $SnO_2$ film (panels c and d).

images show that both the pure and Gd-doped $SnO_2$ films are homogeneous throughout, demanding a uniform Gd doping with no accumulation of Gd for the Gd-doped film. From the SEM image of the 5% Gd-doped $SnO_2$ thin film (inset of Figure 3b), it is also clear that the thin film is nanocrystalline, with prominent grains having an average grain size of ~50 nm. The grains are also very clearly discernable for the Gd-doped $SnO_2$ thin films, compared to that of pure $SnO_2$ thin films, which indicates a better crystalinity of the 5% Gd-doped $SnO_2$ film. This is probably because the doping of trivalent Gd ions, which favors the achievement of better crystallinity in $SnO_2$ films. The energy-dispersive X-ray (EDAX) spectrum of the 5% Gd-doped $SnO_2$ thin films is shown in Figure 4. The Gd concentrations in the thin films quantified by EDAX spectroscopy are found to be 4.87, 1.91, and 0.82 at.% for nominal Gd concentrations of 5, 2, and 1 at.%. The Si K peak originates from the Si substrate on which $SnO_2$ films are deposited, whereas the Au K signal appears from the gold layer coated on the $SnO_2$ films (which was required for the SEM investigation).

Figure 5 shows the atomic force microscopy (AFM) and the corresponding magnetic force microscopy (MFM) images of the pure and 5% Gd-doped $SnO_2$ films at a lift height of ~300 nm over a scan size of 2 $\mu$m × 2 $\mu$m. It is evident from Figure 5 that the MFM features of the films are different from the topography of the films. It is found that the MFM amplitude image shows some course grainlike domain structures, where the bright and dark contrast of domains correspond to high concentrations of positive and negative poles, respectively. The domain configurations are also different for the pure and 5% Gd-doped $SnO_2$ films. The grainlike domain structures are more prominent and vivid in the case of the pure $SnO_2$ nanocrystalline thin films (see Figure 5b), compared to the 5% Gd-doped $SnO_2$ film (see Figure 5d). In the case of 5% Gd-doped $SnO_2$ films, the bright grainlike domains are less in number, and they are random and far apart from each other. Therefore, the observed regular distribution of the bright and dark grainlike magnetic domains in the pure $SnO_2$ thin film is an indication of long-range magnetic ordering in it over the Gd-doped $SnO_2$ films.[35−37]

Figure 6 shows the field dependent magnetization $M$ (H) measurements of pure and Gd-doped $SnO_2$ thin films. Interestingly, the pure $SnO_2$ thin film exhibits a clear hysteresis loop, which indicates that the pristine $SnO_2$ thin films are ferromagnetic at room temperature (Figure 6a) as well as at

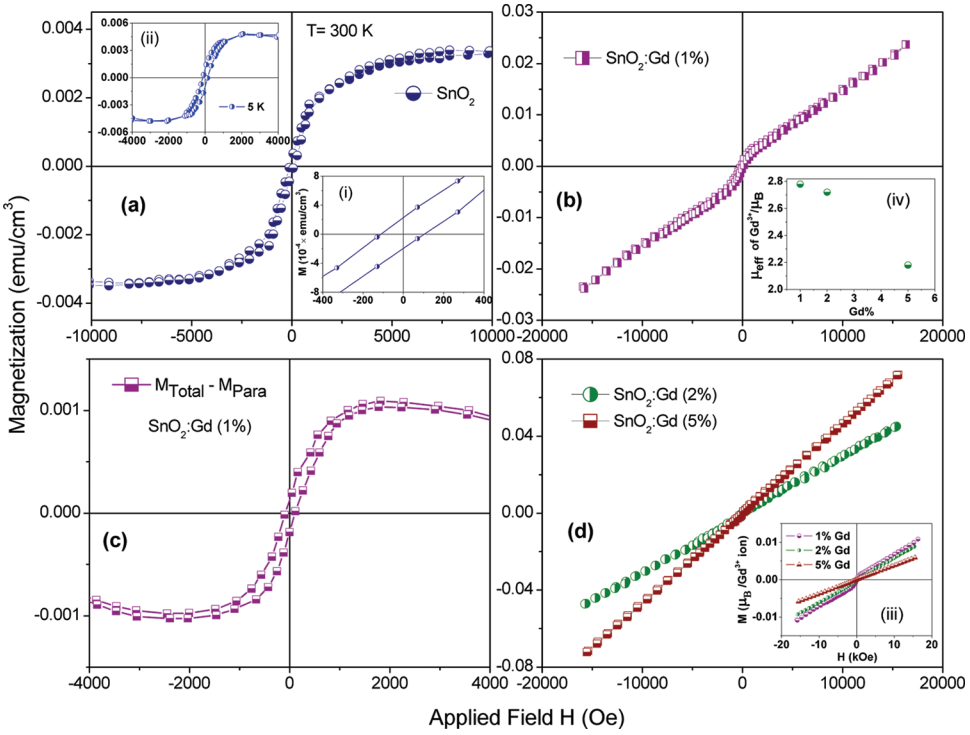


**Figure 6.** Field dependent magnetization ($M$ (H)) loops of (a) the pristine $SnO_2$ thin film at 300 K, (b) 1% Gd-doped $SnO_2$, (c) the ferromagnetic component ($M_{Total} - M_{Para}$) of the 1% Gd-doped film after subtracting the paramagnetic component and (d) the 2% and 5% Gd-doped $SnO_2$ thin films. Insets show (i) the magnetization of pure $SnO_2$ in low field area at 300 K, (ii) the $M-H$ loop of pure $SnO_2$ at 5 K, (iii) the magnetization of Gd-doped films (in units of $\mu_B$ per $Gd^{3+}$ ion), and (iv) the effective magnetic moment ($\mu_{eff}$) of the individual Gd ion in units of Bohr magnetron ($\mu_B$) versus the Gd concentration in the film. (All data presented after correcting the diamagnetic substrate contribution.)

low temperature (inset (ii) of Figure 6a). A significant amount of coercivity ($H_c \approx 110$ and 125 Oe at 300 and 5 K, respectively) is observed in the case of pure $SnO_2$ film, which ensures the FM nature. The saturation magnetization ($M_s$) and retentivity ($M_r$) are found to be $3.4 \times 10^{-3}$ and $2.2 \times 10^{-4}$ emu/cm$^3$, respectively, at 300 K and $4.6 \times 10^{-3}$ and $9.8 \times 10^{-4}$ emu/cm$^3$, respectively, at 5 K. This type of ferromagnetic response in other pristine oxides has also been reported earlier.[19−21] On the other hand, it is quite interesting to observe that Gd-doped $SnO_2$ films show a linear $M-H$ behavior (see Figures 6b and d), which indicates that a dominant paramagnetic ordering is present in the Gd-doped films. In the case of the 1% Gd-doped film, a curvature is observed near the origin (Figure 6b), which indicates that a ferromagnetic component is superimposed over a strong paramagnetic background. Therefore, we have subtracted the strong paramagnetic component ($M_{Para}$) from the total moment ($M_{Total}$) and plotted the residual component ($M_{Total} - M_{Para}$) in Figure 6c, which shows the clear hysteresis-type behavior with a coercivity of $H_C \approx 95$ Oe. The saturation magnetization ($M_s$) is determined to be $1.05 \times 10^{-3}$ emu/cm$^3$, which is much smaller, compared to that of the pure $SnO_2$ film. Therefore, with 1 at.% Gd doping in the $SnO_2$ film, the FM is found to be suppressed subsequently and a large paramagnetic moment is established within the system. For the 2% Gd-doped film, the ferromagnetic component ($M_{Total} - M_{Para}$) is observed to have completely vanished, while the paramagnetic component has been enhanced significantly. Similarly, no FM is found for 5% Gd-doped films either. Therefore, the FM in pure $SnO_2$ film tends to diminish gradually with the increase in Gd doping, and then, over a certain Gd concentration (lying somewhere between 1 and 2 at.%), it completely vanishes. However, the earlier MFM studies also showed an indication of long-range ferromagnetic ordering in the pure $SnO_2$ films, whereas no such observation was found for the 5% Gd-doped film. Note that, although the associated magnetic moment is increased by 1 order of magnitude, because of the insertion of $Gd^{3+}$ ions, which have a localized $f$-shell paramagnetic moment, there is no intrinsic ferromagnetic ordering in the Gd-doped $SnO_2$ films. However, similar results were also obtained by Ney et al.,[17] Xu et al.,[38] and Barla et al.[39] in the case Co-doped ZnO thin films and also in our previous work on the Co-doped $SnO_2$.[15] Recently, a loss of magnetization is also observed in $CeO_2$ thin films[18] with the doping of TM ions. Herein, we estimated the magnetization per $Gd^{3+}$ ion and the effective magnetic moment ($\mu_{eff}$) of the individual Gd ion in units of Bohr magnetron ($\mu_B$), shown in insets (iii) and (iv) of Figure 6, respectively. Note that the magnetization per Gd ion, as well as the $\mu_{eff}$ value, decreases as the Gd concentration increases, which may be due to enhancement of the antiferromagnetic superexchange interaction between $Gd^{3+}$ ions via oxygen ligands. With the increase of Gd concentration in the $SnO_2$ matrix, the average distance between the $Gd^{3+}$ ions should decrease, leading to the enhancement of this type of antiferromagnetic superexchange interaction. The $\mu_{eff}$ value of the $Gd^{3+}$ ion is found to be maximum (2.78 $\mu_B$) in 1% Gd-doped $SnO_2$ film, which is much less than the full moment of the $Gd^{3+}$ ion (7.94 $\mu_B$). Similar results are also observed in the case of Co:ZnO,[10] Co:$SnO_2$,[15] and Gd:ZnO,[40] where the effective moment of the respective TM or RE ion is observed to decrease significantly. This can happen because the moment of the magnetic ions is dependent on the ionic environment[41,42] and ion symmetry within the host matrix. The increase of Gd concentration results in a lattice distortion, which can change the $Gd^{3+}$ site

symmetry as well as the effective magnetic moment of the $Gd^{3+}$ ion.

To understand the magnetic properties in further detail, zero-field-cooled (ZFC) and field-cooled (FC) measurements are also performed for Gd-doped $SnO_2$ films, shown in Figure 7.

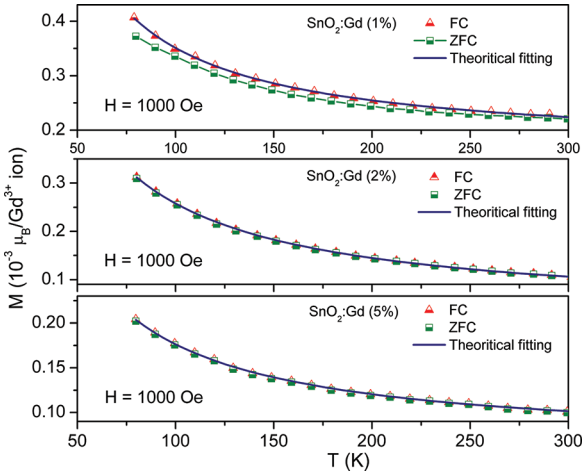


**Figure 7.** Field-cooled/zero-field-cooled (FC–ZFC) plots for all the Gd-doped $SnO_2$ thin films in a constant field of 1000 Oe, along with the theoretical fitting of FC curves according to the modified Curie–Weiss law.

In the case of the 2% and 5% Gd-doped $SnO_2$ films, both ZFC and FC curves (Figures 7b and 7c) trace the same path over the entire range of temperature, which demonstrates the presence of noninteracting paramagnetic moments in the system. However, in the case of the 1% Gd-doped film, the FC curve showed a higher moment than ZFC, which indicates the presence of a ferromagnetic phase. FC curves are also fitted according to the modified Curie–Weiss law:

$$\chi = \frac{m(T)}{H} = \chi_0 + \frac{C}{T + \theta}$$

where $\chi_0$ represents weak nonparamagnetic susceptibility; $C$ is the Curie constant ($C = N\mu^2/(3k)$, where $N$ is the number of magnetic ions per gram, $\mu$ the magnetic moment of the ion, and $k$ the Boltzmann constant), which represents the paramagnetic ion concentration; $T$ is the temperature (in Kelvin); and $\theta$ is the Curie–Weiss temperature, which represents the magnetic exchange interactions between the localized spins. These fits yields $\theta$ values of 4.25, 3.8, and −9.67 K for 5%, 2%, and 1% Gd-doped $SnO_2$ films, respectively. Note that, unlike other films, the 1% Gd-doped film showed negative Curie–Weiss temperature ($\theta$), which demonstrates the existence of a ferromagnetic exchange interaction in this film. The positive $\theta$ value for the 2% and 5% Gd-doped films signifies the existence of the antiferromagnetic exchange interaction between the $Gd^{3+}$ ions. $Gd^{3+}$–$O^{2-}$–$Gd^{3+}$ superexchange interaction might be the possible origin of the antiferromagnetism, whereas the $Gd^{3+}$–$Gd^{3+}$ direct interaction is paramagnetic in nature.

Therefore, the study of the magnetic properties of the pure and Gd-doped $SnO_2$ thin films generates two questions:

(i) Do magnetic ions (such as $Gd^{3+}$) play any role in inducing FM in such oxides? and
(ii) What makes pure $SnO_2$ thin film ferromagnetic?

To address those questions, it is essential to study the intrinsic defects that might be present in $SnO_2$ thin films. Hence, we have performed room-temperature (RT) photoluminescence (PL) measurements, as shown in Figure 8, to investigate the

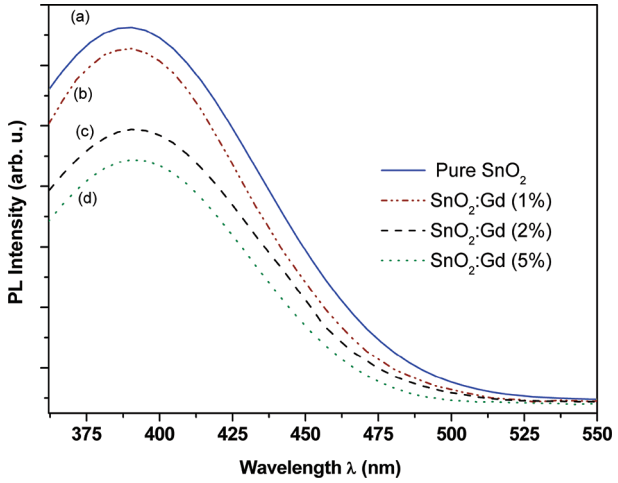


**Figure 8.** Photoluminesence (PL) spectrum of (a) pristine $SnO_2$ thin film and (b) 1%, (c) 2%, and (d) 5% Gd-doped $SnO_2$ thin films.

types of structural defects present in the pure and Gd-doped $SnO_2$ thin films. It is found that, under an excitation of 330-nm light from the Xe source, all the nanocrystalline thin films exhibit an intense broad PL emission band centered at 390 nm (3.17 eV). Since this emission energy (3.17 eV) is much lower than the energy band gap of $SnO_2$ (3.6 eV), the visible emission cannot be assigned to the direct recombination of conduction electron to the holes in valence band; intsead, they are assigned to the defect-related emission. The strong blue emission from the thin films might be related to the inherent crystalline defects induced during their growth.[43−45] It is important to note that the broad nature of the PL emission band clearly indicates that the luminescence should have originated from the multiple sources rather than a single source, because the PL band can be well-fitted with the multiple PL peaks. It is reported that the $SnO_2$ nanostructures can exhibit emission bands between 400 and 600 nm, because of the presence of different crystalline defects.[46−48] The Sn vacancies ($V_{Sn}$) and oxygen vacancies ($V_O$) are the main structural defects present in the $SnO_2$ nanostructures responsible for introducing the defect states in the mid band gap, leading to luminescence in the visible region.[49] Although the formation energy of $V_{Sn}$ is higher than that of $V_O$, it is expected that the concentration of $V_{Sn}$ defects in the $SnO_2$ should be much lower than that of the oxygen vacancies.[21,33] It has been reported that the nanocrystalline $SnO_2$ thin films exhibit intense photoemission at ∼3.13 eV at different temperatures.[50] The blue luminescence from the $SnO_2$ thin films in the wavelength range of 400–450 nm has also been reported by other researchers,[43,51] yet the origin of this PL emission band still has not been understood properly. It is assumed that the PL peaks might be attributed to the defects in the nanocrystal grains,[43,50] or the oxygen vacancy defects,[43,50,51] or even the Sn interstitial ($Sn_i$) defects.[39] However, the broad photoemission peak centered at ∼400 nm is believed to originate because of the electron transition mediated by the $V_O$-related defects in the band gap.[43,50,51] With the energy level of the $V_O$ defects being highly controversial, in this experimen,t


dx.doi.org/10.1021/am300023a | ACS Appl. Mater. Interfaces 2012, 4, 2048–2056

the PL emission peak centered at ~390 nm is attributed to the $V_O$-related defects, mainly singly ionized oxygen vacancy ($F^+$ center or $V_O^+$) defects, which are believed to be the recombination center for the luminescence.[20,29] In our experiment, it is quite expected that the films should contain the $V_O^+$ defects, because the films are deposited in an oxygen-deficient atmosphere. However, here, we cannot also discard the presence of the $V_{Sn}$ defects in the pure and Gd-doped $SnO_2$ films: the cation vacancy defects are also quite obvious in the lattice of the oxide semiconductors. Recently, the cation-vacancy-related defects are attributed to the visible emission as well as to the RTFM in the doped ZnO thin films and nanostructures.[21,52−54] It has been found that the doping of the suitable element can also help in the formation of the cation vacancies in the lattice.[21] It is evident from Figure 8 that the intensity of the PL emission centered at 390 nm is maximum for the pure $SnO_2$ thin film. Therefore, it is expected that the singly ionized oxygen vacancy ($V_O^+$) defect concentration is maximum in the pristine $SnO_2$ nanocrystalline film, compared to the Gd-doped films. However, the decrease of the intensity of the PL emission band with the increase of the Gd concentration in the Gd-doped $SnO_2$ films may be attributed to the considerable attenuation of the oxygen vacancies in the lattice, where the $V_{Sn}$ defects could predominate and the PL emission bands becomes broader in nature with the increase of the Gd concentration in the matrix.

Here, it is important to mention that enough precaution is taken during the preparation of the films to avoid any type of contamination. Nonmagnetic tweezers that have plastic tips are used to transfer the films during different measurements. In fact, no impurities have been detected from XRD and EDAX analysis considering their detection limit. Moreover, we also have tried to exclude any type of instrumental error by conducting the magnetic measurements repeatedly. Therefore, to discuss the origin of FM in pristine $SnO_2$ thin film, it is quite clear from the PL studies that intrinsic defects are playing the key role to induce FM in $SnO_2$. The present PL analysis has shown that structural defects, such as $V_O^+$ defects, are maximum in the pure $SnO_2$ thin film. Here, it is worth mentioning that a single $V_O^+$ defect can generate a localized magnetic moment of ~1.0 $\mu_B$ and when this type of defect ($V_O^+$) concentration goes above the percolation limit, a ferromagnetic exchange interaction can be stabilized,[20,32,45,55] as observed in the pure $SnO_2$ thin film. On the other hand, the $V_O^+$ defect concentration was observed to decrease with increasing Gd doping in $SnO_2$ films. Although the $V_O^+$ defect concentration decreased in the 1% Gd-doped film, still the amount might be sufficient to mediate ferromagnetic interaction in this film. Therefore, the 1% Gd-doped film exhibits a weak FM signature, compared to that of the pure $SnO_2$ film. However, when the Gd concentration exceeds 2 at.%, the $V_O^+$ defect concentration might have fallen below the required percolation limit to sustain long-range ferromagnetic ordering between $V_O^+$ defects and, hence, the destruction of FM. However, the paramagnetic moments associated with the localized $Gd^{3+}$ ions still exist and that is contributing to the total magnetic moments. Previously, we have seen, from the Curie−Weiss fittings, that the exchange interaction exists between $Gd^{3+}$ ions are only the antiferromagnetic type at very low temperatures but not ferromagnetic one. Therefore, we demonstrate that the FM arises only because of the intrinsic structural defects, such as $V_O^+$ defects of $SnO_2$ lattice and, here, the magnetic ions (such as $Gd^{3+}$) have no influence in inducing FM in $SnO_2$ thin films. However, it is important to mention that the Sn vacancy ($V_{Sn}$) defects are also reported to generate localized magnetic moments.[30,31] The previous PL measurements indicate that there might have been some $V_{Sn}$ defects present in the thin films, and they may be low in defect concentration because of their high formation energy.[33] Hence, it is expected that the concentration of the $V_{Sn}$ defects present in the films should be far below the required percolation threshold to mediate long-range ferromagnetic ordering in both $SnO_2$ thin films, because it is not probable to have a considerable amount of $V_{Sn}$ defects in $SnO_2$ without proper defect-engineering. The chance of the formation of $V_O^+$ defects is much easier, because of its low formation energy;[33] in addition, in this work, the formation of $V_O^+$ defects in $SnO_2$ thin films is quite possible, because all the thin films are deposited in an oxygen-deficient atmosphere, where the oxygen:argon ratio is 1:10.

The study of the electrical conductivity and the type of the charge carriers present in the oxide semiconductor thin films can also provide information about the intrinsic nature of the films. In this regard, here, we have investigated the types of charge carriers and the carrier concentrations by Hall measurements and also the electrical conductivity of the pure and Gd-doped $SnO_2$ thin films. The variations of the resistivity ($\rho$), carrier concentration ($n$), Hall coefficient ($R_H$), and mobility ($\mu$) of the $SnO_2$ thin films, relative to the Gd-doping concentration, are shown in Figure 9, and their values are

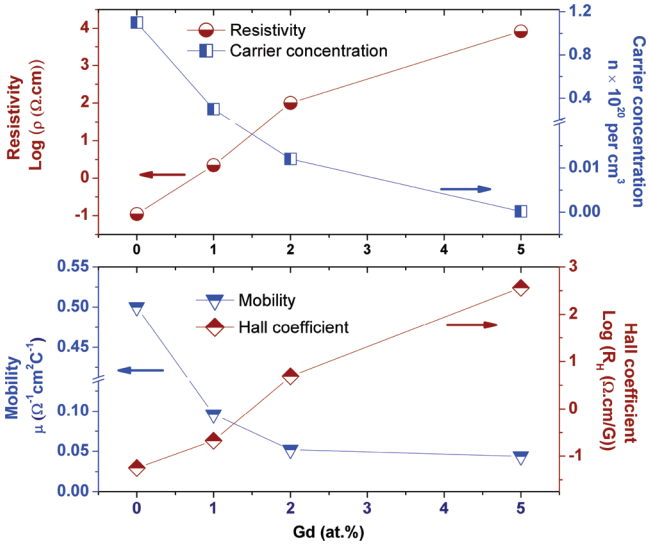


**Figure 9.** Variation of resistivity ($\rho$), carrier concentration ($n$), Hall coefficient ($R_H$), and mobility ($\mu$) of $SnO_2$ thin films with Gd concentration.

summarized in Table 2. The negative value of $R_H$ in the case of the pure $SnO_2$ and 1% Gd-doped thin film indicates $n$-type semiconducting nature, which is due to the presence of oxygen vacancies.[33,56,57] On the other hand, the 2% and 5% Gd-doped $SnO_2$ films show a positive value of $R_H$, which indicates their $p$-type semiconducting behavior. This $n$-type to $p$-type transformation of the pure $SnO_2$ thin film with Gd doping can be understood because of the gradual substitution of $Gd^{3+}$ ions at $Sn^{4+}$ sites, which enhances hole concentration into the $SnO_2$ system. Figure 9 shows that, as the Gd- doping increases in the $SnO_2$ thin film, the electron concentration gradually decreases, which means an increase in hole concentration. The previous PL study also indicates that, with the increase of the Gd

Table 2. Typical Estimated Values of Resistivity ($\rho$), Hall Coefficient ($R_H$), Carrier Concentration ($n$), Mobility of Carriers ($\mu$), and Types of Semiconductors for Pristine and Gd-Doped $SnO_2$ Thin Films

| thin film | resistivity, $\rho$ ($\Omega$ cm) | Hall coefficient, $R_H$ ($\Omega$ cm/G) | carrier concentration, $n$ ($cm^{-3}$) | mobility, $\mu$ ($\Omega^{-1}cm^2C^{-1}$) | type of semiconductor |
|---|---|---|---|---|---|
| $SnO_2$ | $1.1 \times 10^{-1}$ | $-5.6 \times 10^{-2}$ | $1.1 \times 10^{20}$ | 0.50 | *n*-type |
| $SnO_2$:Gd (1%) | 2.2 | $-2.1 \times 10^{-1}$ | $3.0 \times 10^{19}$ | $9.6 \times 10^{-1}$ | *n*-type |
| $SnO_2$:Gd (2%) | $10^2$ | +4.87 | $1.2 \times 10^{18}$ | $5.2 \times 10^{-1}$ | *p*-type |
| $SnO_2$:Gd (5%) | $8.3 \times 10^3$ | $+3.6 \times 10^2$ | $1.7 \times 10^{16}$ | $4.4 \times 10^{-1}$ | *p*-type |

concentration in the $SnO_2$ film, the $V_{Sn}$ defects could predominate as the concentration of $V_O$ defects decreases significantly. The acceptor-type $V_{Sn}$ defects may also contribute to the *p*-type nature of the doped $SnO_2$ thin films. The *n*-type conductivity of the pure $SnO_2$ thin film signifies that the film is enriched with the $V_O$ defects, whereas the doping of the $Gd^{3+}$ ion at the $Sn^{4+}$ site can modify the multivalence of tin probably through the $Sn_i$ population and, thus, the donor level inside the conduction band. As a result, the resistivity ($\rho$) of the pure $SnO_2$ thin film increases as the Gd-doping concentration increases. The 5% Gd-doped $SnO_2$ thin film becomes the most resistive one ($\rho = 8.3 \times 10^3$ $\Omega$ cm). The carrier concentration ($n$) is found to be on the order of $1.1 \times 10^{20}$ $cm^{-3}$ in the pure $SnO_2$ thin film, and it decreases monotonically as the Gd concentration increases. The mobility ($\mu$) of the charge carriers also decreases with Gd doping and is quite expected, since the mobility of holes is less than that of electrons.

## 4. CONCLUDING REMARKS

In summary, we have successfully studied the role of structural defects in inducing ferromagnetism (FM) in pristine $SnO_2$ thin films and the effects of Gd doping on the magnetic, photoluminescence (PL), and electrical conduction of $SnO_2$ nanocrystalline thin films. Only the pristine $SnO_2$ thin film exhibits FM at both room temperature (RT) and low temperature; the FM signature in pure $SnO_2$ film is found to be suppressed initially with low Gd doping but is completely destroyed at higher dopant concentrations. The magnetic force microscopy (MFM) study indicates long-range magnetic ordering in pure $SnO_2$ films at RT. The PL spectra reveals the presence of large numbers of $V_O^+$ defects, which are found to be responsible for the observed FM in *n*-type pristine $SnO_2$ thin films. The studies indicate that the doping of Gd ions at Sn sites reduces the $V_O^+$ defect concentration significantly and makes the films highly resistive and *p*-type, whereas the pure $SnO_2$ film is highly conductive and *n*-type in nature. Although Gd ions introduce localized paramagnetic moments, still no long-range ferromagnetic ordering is observed in the Gd-doped $SnO_2$ thin films. The result signifies that magnetic ions such as Gd have little influence in inducing FM in $SnO_2$ thin films. Our work will certainly help to overcome the controversy about the origin of ferromagnetism in such magnetic ions-doped wide-band-gap oxide semiconductors.

## AUTHOR INFORMATION

### Corresponding Author

*Phone: +91 (033) 2335 5706-8. Fax: +91 (033) 2335 3477. E-mail: shyam@bose.res.in, sghoshphysics@gmail.com (S.G.).

### Notes

The authors declare no competing financial interest.

## ACKNOWLEDGMENTS

The work is supported by the CSIR-funded project 03(1178)/10/EMR-II. One of the authors (S.G.) thanks the Council of Scientific and Industrial Research (CSIR), Government of India, for providing financial support through a research fellowship. The authors also thank Dr. D. Das (UGC-DAE Consortium for Scientific Research, Kolkata) for providing the SQUID measurement facility.

## REFERENCES

(1) Ohho, H. *Science* **1998**, *281*, 951−955.
(2) Prinz, G. A. *Science* **1998**, *282*, 1660−1663.
(3) Dietl, T.; Ohno, H.; Matsukura, F.; Cibert, J.; Ferrand, D. *Science* **2000**, *287*, 1019−1022.
(4) Coey, J. M. D.; Douvalis, A. P.; Fitzgerald, C. B.; Venkatesan, M. *Appl. Phys. Lett.* **2004**, *84*, 1332.
(5) Punnoose, A.; Hays, J.; Gopal, V.; Shutthanandan, V. *Appl. Phys. Lett.* **2004**, *85*, 1559.
(6) Dakhel, A. A.; El-Hilo, M. *J. Appl. Phys.* **2010**, *107*, 123905.
(7) Mohan Kant, K.; Chandrasekaran, K.; Ogale, S. B.; Venkatesan, T.; Sethupathi, K.; Rao, M. S. R. *J. Appl. Phys.* **2005**, *97*, 10A925.
(8) Griffin, K. A.; Pakhomov, A. B.; Wang, C. M.; Heald, S. M.; Krishnan, K. M. *Phys. Rev. Lett.* **2005**, *94*, 157204.
(9) Lee, H.-J.; Jeong, S. Y.; Hwang, J.-Y.; Cho, C. R. *Europhys. Lett.* **2003**, *64*, 797−802.
(10) Ghosh, S.; Mandal, K. *J. Magn. Magn. Mater.* **2010**, *322*, 1979−1984.
(11) Ghosh, S.; Mandal, M.; Mandal, K. *J. Magn. Magn. Mater.* **2011**, *323*, 1083−1087.
(12) Kaspar, T. C.; Heald, S. M.; Wang, C. M.; Bryan, J. D.; Droubay, T.; Shutthanandan, V.; Thevuthasan, S.; Mccready, D. E.; Kellock, A. J.; Gamelin, D. R.; Chambers, S. A. *Phys. Rev. Lett.* **2005**, *95*, 217203.
(13) Ogale, S. B.; Choudhary, R. J.; Buban, J. P.; Lofland, S. E.; Shinde, S. R.; Kale, S. N.; Kulkarni, V. N.; Higgins, J.; Lanci, C.; Simpson, J. R.; Browning, N. D.; Das Sarma, S.; Drew, H. D.; Greene, R. L.; Venkatesan, T. *Phys. Rev. Lett.* **2003**, *91*, 077205.
(14) Liu, X. F.; Yua, R. H. *J. Appl. Phys.* **2007**, *102*, 083917.
(15) Ghosh, S.; De Munshi, D.; Mandal, K. *J. Appl. Phys.* **2010**, *107*, 123919.
(16) Zunger, A.; Lany, S. *Physics* **2010**, *3*, 53.
(17) Ney, A.; Ollefs, K.; Ye, S.; Kammermeier, T.; Ney, V.; Kaspar, T. C.; Chambers, S. A.; Wilhelm, F.; Rogalev, A. *Phys. Rev. Lett.* **2008**, *100*, 157201.
(18) Fernandes, V.; Schio, P.; de Oliveira, A. J. A.; Schreiner, W. H.; Varalda, J.; Mosca, D. H. *J. Appl. Phys.* **2011**, *110*, 113902.
(19) Venkatesan, M.; Fitzgerald, C. B.; Coey, J. M. D. *Nature* **2004**, *430*, 630.
(20) Sundaresan, A.; Bhargavi, R.; Rangarajan, N.; Siddesh, U.; Rao, C. N. R. *Phys. Rev. B* **2006**, *74*, 161306.
(21) Ghosh, S.; Khan, G. G.; Das, B.; Mandal, K. *J. Appl. Phys.* **2011**, *109*, 123927.
(22) Pemmaraju, C. D.; Sanvito, S. *Phys. Rev. Lett.* **2005**, *94*, 217205.
(23) Elfimov, I. S.; Yunoki, S.; Sawatzky, G. A. *Phys. Rev. Lett.* **2002**, *89*, 216403.
(24) Coey, J. M. D.; Venkatesan, M.; Fitzgerald, C. B. *Nat. Mater.* **2005**, *4*, 173.
(25) Khan, G. G.; Ghosh, S.; Mandal, K. *J. Solid State Chem.* **2012**, *186*, 278−282.

(26) Kumar, E. S.; Venkatesh, S.; Rao, M. S. R. *Appl. Phys. Lett.* **2010**, *96*, 232504.
(27) Iqbal, J.; Wang, B.; Liu, X.; Yu, D.; He, B.; Yu, R. *New J. Phys.* **2009**, *11*, 063009.
(28) Philip, J.; Punnoose, A.; Kim, B. I.; Reddy, K. M.; Layne, S.; Holmes, J. O.; Satpati, B.; Leclair, P. R.; Santos, T. S.; Moodera, J. S. *Nat. Mater.* **2006**, *5*, 298.
(29) Xing, G. Z.; Yi, J. B.; Wang, D. D.; Liao, L.; Yu, T.; Shen, Z. X.; Huan, C. H. A.; Sum, T. C.; Ding, J.; Wu, T. *Phys. Rev. B* **2009**, *79*, 174406.
(30) Bouzerar, G.; Ziman, T. *Phys. Rev. Lett.* **2006**, *96*, 207602.
(31) Rahman, G.; Garcia-Suarez, V. M.; Hong, S. C. *Phys. Rev. B* **2008**, *78*, 184404.
(32) Wang, H.; Yan, Y.; Li, K.; Du, X.; Lan, Z.; Jin, H. *Phys. Status Solidi B* **2010**, *247*, 444.
(33) Kiliç, Ç.; Zunger, A. *Phys. Rev. Lett.* **2002**, *88*, 095501.
(34) Mohan Kant, K.; Chandrasekaran, K.; Ogale, S. B.; Venkatesan, T.; Rao, M. S. R. *J. Appl. Phys.* **2005**, *97*, 10A925.
(35) Herng, T. S.; Wong, M. F.; Qi, D.; Yi, J.; Kumar, A.; Huang, A. F.; Kartawidjaja, C.; Smadici, S.; Abbamonte, P.; Sánchez-Hanke, C.; Shannigrahi, S.; Xue, J. M.; Wang, J.; Feng, Y. P.; Rusydi, A.; Zeng, K.; Ding, J. *Adv. Mater.* **2011**, *23*, 1635−1640.
(36) Philip, J.; Punnoose, A.; Kim, B. I.; Reddy, K. M.; Layne, S.; Holmes, J. O.; Satpati, B.; Leclair, P. R.; Santos, T. S.; Moodera, J. S. *Nat. Mater.* **2006**, *5*, 298.
(37) Jeon, H. C.; Jeong, Y. S.; Kang, T. W.; Kim, T. W.; Chung, K. J.; Chung, K. J.; Jhe, W.; Song, S. A. *Adv. Mater. (Weinheim, Ger.)* **2002**, *14*, 1725.
(38) Xu, Q.; Zhou, S.; Marko, D.; Potzger, K.; Fassbender, J.; Vinnichenko, M.; Helm, M.; Hochmuth, H.; Lorenz, M.; Grundmann, M.; Schmidt, H. *J. Phys. D: Appl. Phys.* **2009**, *42*, 085001.
(39) Barla, A.; Schmerber, G.; Beaurepaire, E.; Dinia, A.; Bieber, H.; Colis, S.; Scheurer, F.; Kappler, J. P.; Imperia, P.; Nolting, F.; Wilhelm, F.; Rogalev, A.; Müller, D.; Grob, J. J. *Phys. Rev. B* **2007**, *76*, 125201.
(40) Dakhel, A. A.; El-Hilo, M. *J. Appl. Phys.* **2010**, *107*, 123905.
(41) Sakamoto, N. *J. Phys. Soc. Jpn.* **1962**, *17*, 99.
(42) Kumagai, H.; Oka, Y.; Kawata, S.; Ohba, M.; Inoue, K.; Kurmoo, M.; Okawa, H. *Polyhedron* **2003**, *22*, 1917.
(43) Jeong, J.; Choi, S. P.; Chang, C. I.; Shin, D. C.; Park, J. S.; Lee, B.-T.; Park, Y.-J.; Song, H.-J. *Solid State Commun.* **2003**, *127*, 595−597.
(44) Gu, F.; Wang, S. F.; Song, C. F.; Lu, M. K.; Qi, Y. X.; Zhou, G. J.; Xu, D.; Yuan, D. R. *Chem. Phys. Lett.* **2003**, *372*, 451−454.
(45) Xing, G.; Wang, D.; Yi, J.; Yang, L.; Gao, M.; He, M.; Yang, J.; Ding, J.; Chien Sum, T.; Wu, T. *Appl. Phys. Lett.* **2010**, *96*, 112511.
(46) He, H.; Wu, T. H.; Hsin, C. L.; Li, K. M.; Chen, L. J.; Chueh, Y. L.; Chou, L. J.; Wang, Z. L. *Small* **2006**, *2*, 116.
(47) Luo, S.; Fan, J.; Liu, W.; Zhang, M.; Song, Z.; Lin, C.; Wu, X.; Chu, P. K. *Nanotechnology* **2006**, *17*, 1695.
(48) Luo, S.; Chu, P. K.; Liu, W.; Zhang, M.; Lin, C. *Appl. Phys. Lett.* **2006**, *88*, 183112.
(49) Zhu, W.; Wang, W.; Xu, H.; Shi, J. *Mater. Chem. Phys.* **2006**, *99*, 127.
(50) Kim, T. W.; Lee, D. U.; Yoon, Y. S. *J. Appl. Phys.* **2000**, *88*, 3759.
(51) Gu, F.; Wang, S. F.; Lu, M. K.; Cheng, X. F.; Liu, S. W.; Zhou, G. J.; Xu, D.; Yuan, D. R. *J. Cryst. Growth* **2004**, *262*, 182−185.
(52) Yi, J. B.; Lim, C. C.; Xing, G. Z.; Fan, H. M.; Van, L. H.; Huang, S. L.; Yang, K. S.; Huang, X. L.; Qin, X. B.; Wang, B. Y.; Wu, T.; Wang, L.; Zhang, H. T.; Gao, X. Y.; Liu, T.; Wee, A. T. S.; Feng, Y. P.; Ding, J. *Phys. Rev. Lett.* **2010**, *104*, 137201.
(53) Li, Y.; Deng, R.; Yao, B.; Xing, G.; Wang, D.; Wu, T. *Appl. Phys. Lett.* **2010**, *97*, 102506.
(54) Zhang, B. Y.; Yao, B.; Li, Y. F.; Liu, A. M.; Zhang, Z. Z.; Li, B. H.; Xing, G. Z.; Wu, T.; Qin, X. B.; Zhao, D. X.; Shan, C. X.; Shen, D. Z. *Appl. Phys. Lett.* **2011**, *99*, 182503.
(55) Podila, R.; Queen, W.; Nath, A.; Arantes, J. T.; Schoenhalz, A. L.; Fazzio, A.; Dalpian, G. M.; He, J.; Hwu, S. J.; Skove, M. J.; Rao, A. M. *Nano Lett.* **2010**, *10*, 1383.
(56) Du, X.; Du, Y.; George, S. M. *J. Vac. Sci. Technol. A* **2005**, *23*, 581.
(57) Yan, H.; Chen, G. H.; Man, W. K.; Wong, S. P.; Kwok, R. W. M. *Thin Solid Films* **1998**, *326*, 88.